Sufficient oxygen for animal respiration 1,400 million years ago

Shuichang Zhang[a,1], Xiaomei Wang[a], Huajian Wang[a], Christian J. Bjerrum[b,c], Emma U. Hammarlund[d,e], M. Mafalda Costa[f,g], James N. Connelly[f,g], Baomin Zhang[a], Jin Su[a], and Donald E. Canfield[d,e,1]

[a]Key Laboratory of Petroleum Geochemistry, Research Institute of Petroleum Exploration and Development, China National Petroleum Corporation, Beijing 100083, China; [b]Department of Geosciences and Natural Resource Management, Section of Geology, University of Copenhagen, DK-1350 Copenhagen, Denmark; [c]The Nordic Center for Earth Evolution at the Department of Geosciences and Natural Resource Management, Section of Geology, University of Copenhagen, DK-1350 Copenhagen, Denmark; [d]Institute of Biology, University of Southern Denmark, DK-5230 Odense, Denmark; [e]The Nordic Center for Earth Evolution at the Institute of Biology, University of Southern Denmark, DK-5230 Odense, Denmark; [f]Centre for Star and Planet Formation, University of Copenhagen, DK-1350 Copenhagen, Denmark; and [g]Natural History Museum of Denmark, University of Copenhagen, DK-1350 Copenhagen, Denmark

Contributed by Donald E. Canfield, November 27, 2015 (sent for review November 2, 2015; reviewed by Lee Kump and Jennifer Morford)

The Mesoproterozoic Eon [1,600–1,000 million years ago (Ma)] is emerging as a key interval in Earth history, with a unique geochemical history that might have influenced the course of biological evolution on Earth. Indeed, although this time interval is rather poorly understood, recent chromium isotope results suggest that atmospheric oxygen levels were <0.1% of present levels, sufficiently low to have inhibited the evolution of animal life. In contrast, using a different approach, we explore the distribution and enrichments of redox-sensitive trace metals in the 1,400 Ma sediments of Unit 3 of the Xiamaling Formation, North China Block. Patterns of trace metal enrichments reveal oxygenated bottom waters during deposition of the sediments, and biomarker results demonstrate the presence of green sulfur bacteria in the water column. Thus, we document an ancient oxygen minimum zone. We develop a simple, yet comprehensive, model of marine carbon–oxygen cycle dynamics to show that our geochemical results are consistent with atmospheric oxygen levels >4% of present-day levels. Therefore, in contrast to previous suggestions, we show that there was sufficient oxygen to fuel animal respiration long before the evolution of animals themselves.

atmosphere | Mesoproterozoic | oxygen minimum zone | trace metals | biomarkers

Some aspects of the history of atmospheric oxygen on Earth are well understood. For example, before about 2,300 million years ago (Ma), atmospheric oxygen was likely less than 0.001% of present atmospheric levels (PAL) (1, 2), whereas, after about 550 Ma, levels have been greater than about 20% PAL (3–5), sufficient to sustain large-animal respiration. The intervening history, however, has been both poorly studied and poorly constrained. This history is of critical importance as it allows one to establish possible links between changing oxygen levels and animal evolution, where molecular clock estimates showing an evolution of crown-group metazoans (including the ancestors of modern Porifera and Placozoa) sometime during the Cryogenian Period (720–635 Ma) (6, 7). Indeed, there is a long-standing suggestion that rising atmospheric oxygen concentrations in the late Neoproterozoic Eon (1,000–542 Ma) (8–11) enabled animal respiration, thus explaining the timing of animal evolution.

The oxygen levels required for early animal respiration were lower than those needed to sustain large motile animals and were probably ≤1% PAL (10, 12, 13). Recent chromium isotope results suggest oxygen levels of <0.1% PAL through the Mesoproterozoic Eon (1,600–1,000 Ma) and until about 700 Ma, when rising levels then spurred animal evolution (11). In contrast, we present evidence that oxygen was ≥3.8% PAL at 1,390 Ma, sufficient to fuel early animal respiration.

Study Site and Sample Collection

The Xiamaling Formation (see Fig. S1) was deposited below storm wave base in a tropical setting between 10°N and 30°N (14, 15). Pre-Xiamaling sediments were deposited on a passive margin, but occasional ash layers in the Xiamaling Formation have led to suggestions of a back-arc setting (15). Sediments of the Xiamaling Formation, however, are highly laminated with no evidence for mass flows or turbidites, and volcanoclastics are rare. Therefore, deposition in a tectonically quiet environment is indicated, consistent with continued deposition on a passive margin. There is also no evidence for storm wave interaction with the sediment, so a water depth of >100 m is likely. The sediment package was never heated to above 90 °C, thus preserving organic biomarkers (16). High-precision zircon data yield an age of 1,384.4 ± 1.4 Ma for a tuff layer 210 m below the top of the formation and 1,392.2 ± 1.0 Ma for a bentonite layer 52 m below the tuff layer (16).

As one of our objectives was to study biomarker distributions within the Xiamaling sediments, most of our data come from cores obtained with fresh water as drilling fluid. In some cases, we compared our inorganic geochemical results to results obtained from outcrop samples, where the outer weathered layer was first removed. Details of our sediment sampling procedures and analytical methods are described in *Supporting Information*.

Significance

How have environmental constraints influenced the timing of animal evolution? It is often argued that oxygen first increased to sufficient levels for animal respiration during the Neoproterozoic Eon, 1,000 million to 542 million years ago, thus explaining the timing of animal evolution. We report geochemical evidence for deep-water oxygenation below an ancient oxygen minimum zone 1,400 million years ago. Oceanographic modeling constrains atmospheric oxygen to a minimum of ∼4% of today's values, sufficient oxygen to have fueled early-evolved animal clades. Therefore, we suggest that there was sufficient atmospheric oxygen for animals long before the evolution of animals themselves, and that rising levels of Neoproterozoic oxygen did not contribute to the relatively late appearance of animal life on Earth.

Author contributions: S.Z., X.W., H.W., E.U.H., J.N.C., and D.E.C. designed research; S.Z., X.W., H.W., C.J.B., E.U.H., M.M.C., B.Z., J.S., and D.E.C. performed research; S.Z., X.W., H.W., C.J.B., M.M.C., J.N.C., and D.E.C. analyzed data; C.J.B. and D.E.C. developed and performed O_2 model calculation; and S.Z., X.W., C.J.B., E.U.H., J.N.C., and D.E.C. wrote the paper.

Reviewers: L.K., Pennsylvania State University; and J.M., Franklin and Marshall.

The authors declare no conflict of interest.

Freely available online through the PNAS open access option.

[1]To whom correspondence may be addressed. Email: sczhang@petrochina.com.cn or dec@biology.sdu.dk.

This article contains supporting information online at www.pnas.org/lookup/suppl/doi:10.1073/pnas.1523449113/-/DCSupplemental.

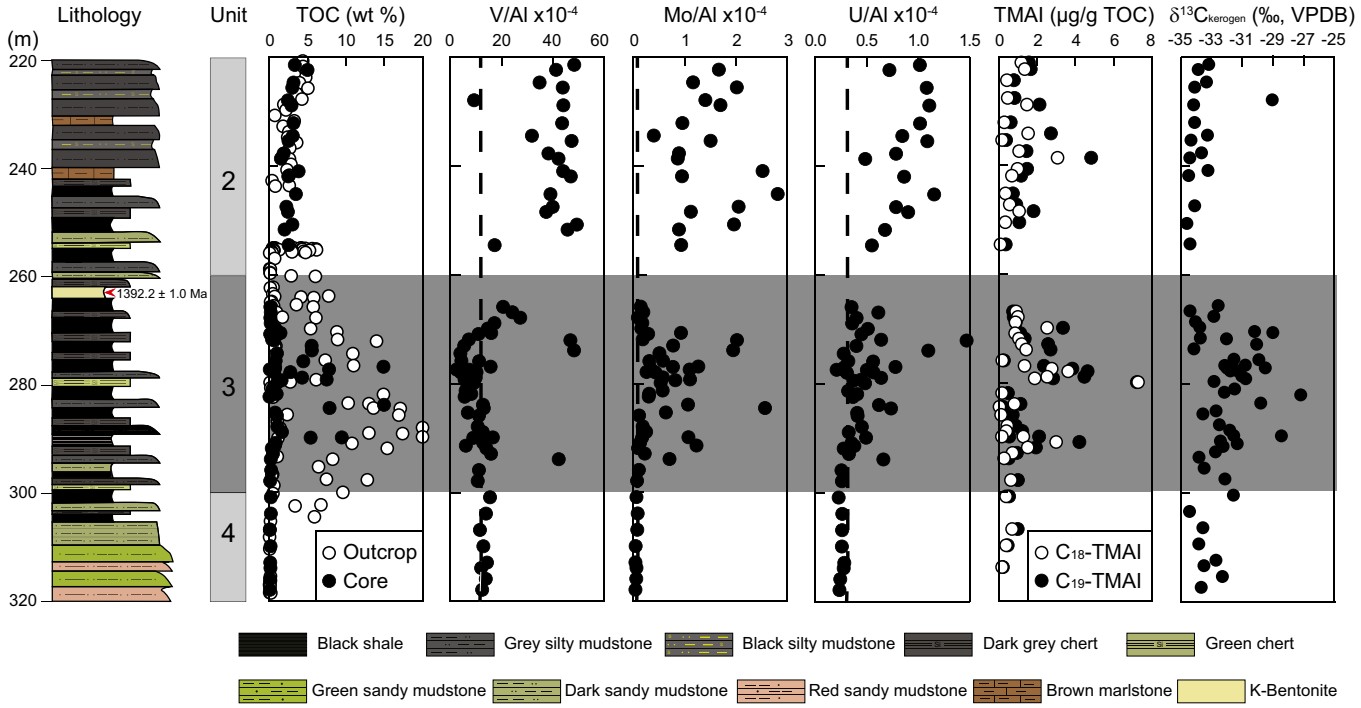

Fig. 1. Geochemistry, biomarker, and $\delta^{13}C$ of kerogen for the Xiamaling Formation from the top of unit 4 to the bottom of unit 2. TOC, from both the core and outcrop samples are presented. Data include both black shales and other sediment types like cherts. Vertical dotted lines represent concentration ratios relative to crustal average (see *Supporting Information* and Tables S1 and S2).

Evidence for Bottom Water Oxygenation

In a zone from 260 to 300 m depth, shales with high total organic carbon (TOC) alternate with low-TOC cherts (Fig. 1 and Fig. S2). These sediments are distinct from the low-TOC sediments deposited below this interval and the intermediate-TOC sediments deposited above. The high-TOC zone is best expressed in outcrop samples, due to the low sample recovery of shales during coring (Fig. 1). The alteration between the high-TOC shales and low-TOC cherts likely represents orbitally forced changes in trade wind intensity, as this influenced the strength of coastal upwelling (16).

The high-TOC shales within the high-TOC zone, and particularly in the depth range of 270–295 m, are enriched in the redox-sensitive elements molybdenum (Mo) and uranium (U) (Fig. 1 and Fig. S2) but are either depleted or unenriched in vanadium (V). The gray shales in this interval show small to negligible enrichments in Mo and U, but, like the black shales, many also show depletion in V. Our focus, however, will be on the geochemical environment surrounding black shale deposition. In modern environments, V is commonly released from sediments depositing under low-oxygen (but still oxygenated) conditions (17, 18) and under normal bottom water oxygen levels where oxygen only penetrates a few millimeters into the sediment. Vanadate is transported to sediments as the vanadate ion $[H_2V(VI)O_4^-]$ adsorbed onto Mn oxides. The vanadate ion is released as the Mn oxides are reduced to Mn^{2+} (18), and, where oxygen is limiting, Mn oxides do not readily reform at the sediment surface (18–20), allowing vanadate to escape to the overlying water.

Vanadate is also released into anoxic waters following Mn oxide reduction, but in the absence of oxygen, the vanadate is reduced to the vanadyl form $[V(IV)O^{2+}]$ (18). This form is highly surface-reactive and removed to the sediment together with vanadyl ions formed from vanadate ions transported across the chemocline into the anoxic waters. Thus, in oxygen minimum zones (OMZs) where anoxic waters overlay sediments, and in euxinic basins, V is enriched together with Mo and U (17, 21–23). In summary, coenrichments of V, Mo, and U occur under anoxic water column conditions, whereas V release from sediments only occurs under bottom water oxygenation (see *Supporting Information* for further discussion).

Thus, trace metal patterns demonstrate bottom water oxygenation during deposition of unit 3 of the Xiamaling Formation. Our results complement a previous study from the 1,410 Ma Kaltasy Formation, Volgo-Ural region, Russia, where Fe speciation and trace metal abundances (these sediments also indicate V release relative to crustal average values) indicate bottom water oxygenation in sediments deposited deeper than storm wave base (likely >150 m depth) (24).

Evidence for an Oxygen Minimum Zone Setting

The chemical environment of the Xiamaling Formation is further constrained by exploring the abundance of 2,3,6-trimethyl aryl isoprenoids (2,3,6-TMAI). These biomarkers are breakdown products of isorenieratane, whose precursors are isorenieratene and β-isorenieratene, which are themselves carotenoid pigments associated with "brown" strains of green sulfur bacteria (GSB) (*Chlorobiaceae*) (25). These organisms are obligate anaerobic phototrophs that frequent modern and ancient sulfidic (and likely also ferruginous) water columns, using the oxidation of sulfide and ferrous iron to gain energy for building cell biomass (26–30). Elevated abundances of 2,3,6-TMAI's (Fig. 1 and Figs. S3 and S4) suggest that phototrophic low-light-adapted GSB populations occupied the Xiamaling water column during much of unit 3 deposition. Thus, biomarker evidence, combined with trace metal dynamics, suggest that unit 3 of the Xiamaling Formation deposited in a true OMZ setting with deep oxygenated water overlain by anoxic water with either H_2S or Fe^{2+} in the photic zone.

There is some evidence, however, that β-isorenieratane can form from the late diagenetic aromatization of partially hydrogenated β-carotene (31), with the β-carotene sourced from algae

or cyanobacteria. The source of β-isorenieratane, and ultimately the 2,3,6-TMAIs, can, in principle, be tested through the $\delta^{13}C$ of the 2,3,6-TMAI compounds as GSB produce relatively ^{13}C-enriched biomass through the reductive citric acid cycle in carbon fixation (see review in ref. 32). Unfortunately, we were unable to measure the isotopic compositions of the 2,3,6-TMAIs, but the $\delta^{13}C$ of insoluble organic matter (kerogen) tends to heavier values in sync with peak abundances of C_{18}-TMAI or C_{19}-TMAI (Fig. 1). This observation is consistent with the addition of GSB biomass to the carbon pool. Therefore, we are confident that our C_{18}-TMAI and C_{19}-TMAI biomarkers represent the presence of GSB in the ancient Xiamaling Formation water column. We note, however, that although illuminating the geochemical environment, the recognition of an OMZ setting is not critical to constraining atmospheric oxygen concentrations as described immediately below. The most critical point is the recognition that Xiamaling Formation sediments deposited in oxygenated deep waters as constrained from trace metal distributions as described above.

Constraining Atmospheric Oxygen Levels

The presence of oxygenated bottom waters during Xiamaling Formation deposition allows constraints on levels of atmospheric oxygen. The water supplied to OMZs originates as oxygen-saturated surface waters that are mixed during winter months into the thermocline in extratropical latitudes (33). This water loses oxygen to respiration as it flows along isopycnal surfaces to the OMZ (Fig. 2). There is sufficient respiration to consume all of the oxygen flowing to the anoxic portion of an OMZ, but insufficient respiration to consume the oxygen from water flowing to the deeper depths. Our goal is to determine the minimum amounts of atmospheric oxygen required to allow oxygenated waters to persist in these deeper waters. Knowing this, we derive a lower limit for atmospheric oxygen levels, assuming that the upper mixed layer of the ocean was in oxygen equilibrium with the atmosphere.

The oxygen loss to respiration is obtained by combining the transit time of water from its place of ventilation and the rate of oxygen respiration in the water. The transit time of water to the OMZ is approximated by calculating the so-called "water age," which is assessed as the volume of water confined within adjacent layers of constant density (isopycnal surfaces) ratioed by the flux of water into this volume (34). The shortest water ages give the lowest estimates for atmospheric oxygen (see below), and these are found in the South Atlantic, with ages of 5–6 y in the upper ∼100 m of the water column, increasing to about 25 y by 400 m water depth (34). In contrast, water ages in the North Pacific range from 7–20 y in the upper 100 m to well over 100 y by 400 m depth (34). Water ages for restricted and semirestricted marine water bodies generally fall within these ranges (see *Supporting Information* for summary of water ages).

The rate of respiration of marine organic matter decreases as a function of water depth (34), and the rate at a given depth depends on the export flux of organic matter from the upper water column (also called new production), the settling rate of the organic matter, and its degradability. In our modeling, we explored export production values ranging from 10% to 200% of present-day Equatorial Atlantic average values (*Supporting Information*). Of this range, we view 20–150% as a good estimate for the Xiamaling Formation, recognizing that during the Mesoproterozoic Eon, marine carbon isotope values suggest a carbon cycle operating at rates broadly similar to today (35).

We also explored in our modeling a wide range of particle settling rates. We highlight that the settling rates of small, predominantly prokaryote-derived, organic particles 1.39 Ga were likely much lower than today (36) where dense, eukaryote-derived, algal tests and animal-derived fecal material dominate the settling flux (37). Settling velocities of between 1 $m{\cdot}d^{-1}$ and 6 $m{\cdot}d^{-1}$ encompass the range predicted for micrometer-sized planktonic cells, and their aggregates, through a planktonic bloom (38). We focus on this range of settling velocities in interpreting our results.

Organic matter degradability in the modern ocean is assessed from the attenuation of particle-settling fluxes with water depth as revealed through sediment trap experiments. Recent studies, accounting for particle capture efficiency, reveal that upper water column particles degrade more rapidly in low latitudes with higher temperatures than in high latitudes with lower temperatures (39). We least-squares fit the low latitude, the high latitude, and the combined trap data with a continuous reaction model, generating parameters describing the aging of particles as they settle. From these parameters, we calculate the decomposition rate of settling organics with depth as a function of new production and particle settling rate (see *Supporting Information* for details).

In our calculations, new production is equal to the export flux of organic matter at the base of a nominal mixed-layer depth of 50 m, and organic matter is consumed as the particles sink. At a unique water depth for each calculation, the carbon-settling flux matches the burial flux of organic matter into Xiamaling Formation sediments as constrained from precise sediment chronology and sediment TOC content, which varies from 10 wt% to 20 wt% in the black shales (Fig. 1). The rate of oxygen respiration at this depth is then combined with the appropriate water age for the depth to give the total amount of oxygen respired.

Atmospheric oxygen values are calculated from this amount of respired oxygen assuming water saturation with the atmosphere at the temperature corresponding to the diagnosed water depth, where we use the average temperature–depth distribution as found in the tropical to subtropical South Atlantic (see *Supporting Information*). The Xiamaling Formation formed during a prolonged ice-free period of Earth history, and ocean temperatures during this time may have been higher than those in the modern ocean. Higher temperatures ultimately yield higher estimates of atmospheric O_2, as explored below, so focusing on present-day temperatures provides a conservative minimum estimate of atmospheric O_2 concentration. Our estimates of atmospheric O_2 are also minimum values, as our calculation of oxygen levels does not account for excess oxygen in the water as required by the geochemical data.

An example of model results is shown in Fig. 3 *A*–*C*. These results were generated with a Xiamaling Formation TOC content of 15 wt%, organic reactivity from the combined sediment trap data, and water age and temperature depth distributions for the South Atlantic (*Supporting Information*). Within the most likely Mesoproterozoic ranges of new production and particle settling rates (as shown in the outlined box in Fig. 3 *A*–*C*), and for water depths of >100 m (dotted lines in Fig. 3 *A* and *B*), as is likely for the Xiamaling Formation depositional environment,

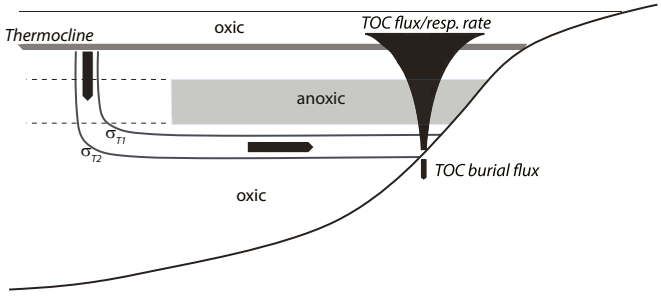

Fig. 2. Cartoon representation of our oxygen respiration model. The cartoon shows the origin of OMZ water at the thermocline, and its transit to the OMZ along layers of constant density σ_t. The cartoon also shows how both the flux of organic carbon and its respiration rate attenuate with depth in the water column. Finally, the cartoon shows our convergence criteria where depth is determined by matching the TOC flux through the water column with the TOC burial flux in Xiamaling Formation sediments.

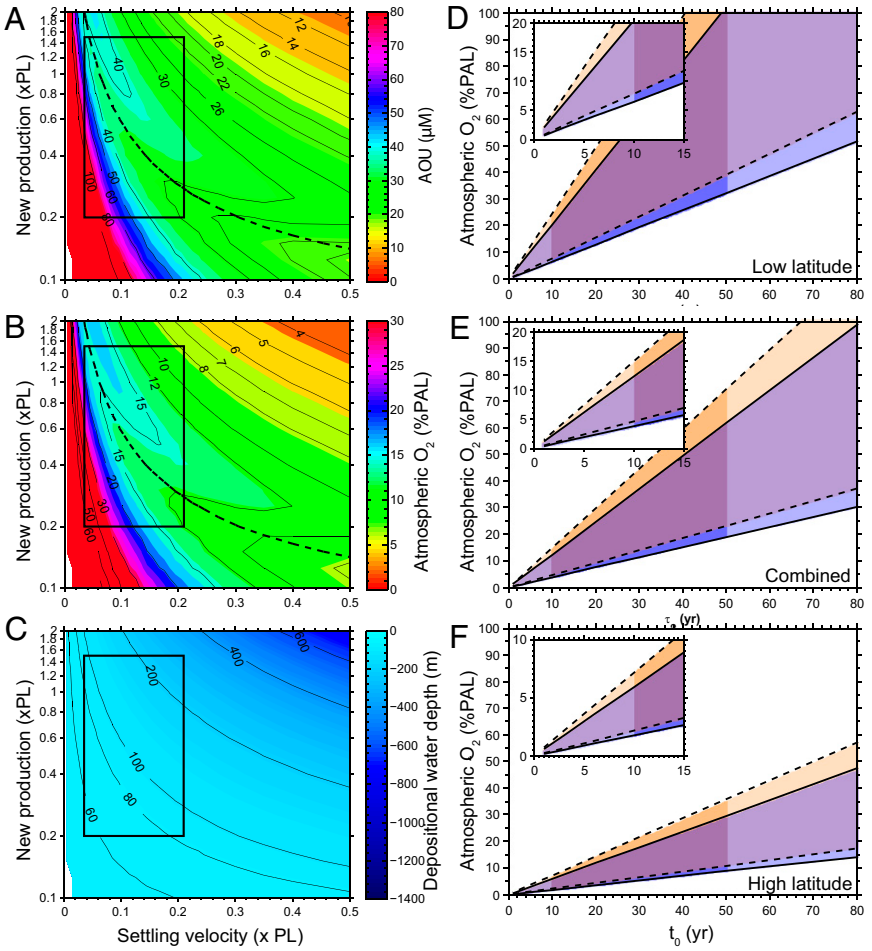

Fig. 3. (*A*) Calculated minimum oxygen utilization (AOU) for water masses circulating to oxygenated waters beneath the anoxic portion of an OMZ. This calculation is calibrated to a Xiamaling Formation organic carbon burial flux calculated from 15 wt% TOC, with organic matter reactivity as calculated from the mean of all sediment trap data, and a temperature–depth distribution as for the present tropical Atlantic Ocean. The black box outlines new production rates ranging from 0.2 to 1.5 times present values (xPL), with the present value as observed in the equatorial Atlantic (*Supporting Information*), and particle settling rates between 1 m·d^{-1} and 6 m·d^{-1} (they are presented as a fraction, xPL-present level, of the diagnosed particle settling rates from the sediment trap data as described in *Supporting Information*). The dotted line indicates the solutions for the 100 m depth contour. (*B*) Values of AOU converted to percent present atmospheric oxygen levels (%PAL) assuming water saturation with air at the temperature for the water depth diagnosed in the calculation. (*C*) Water depths diagnosed by matching the particle settling flux with the burial flux of organic matter into Xiamaling Formation sediments. The stippled line represents water depths of less than 100 m, which we consider unlikely given the deep-water depositional setting of the Xiamaling Formation. (*D*) Sensitivity analyses depicting the high and low oxygen estimates for a series of calculations with variable water residence times (τ_o) assuming low organic matter reactivity as found in modern low latitudes. Calculations with the present-day temperature–depth distributions are shown in blue shades, and calculations with this temperature profile +10 °C are shown in brown. A large overlap is observed. The darkened area outlines the most likely range of water ages. (*E*) As in *D*, but assuming organic matter reactivity from the combined sediment trap data. (*F*) As in *D*, but assuming high organic matter reactivity as found in modern high latitudes. See *Constraining Atmospheric Oxygen Levels* and Figs. S5–S8 and Tables S3–S7 for details.

our calculations show oxygen consumption of between about 21 μM and 40 μM, translating into minimum atmospheric oxygen levels of 8–15% PAL.

Variations in water age, organic matter reactivity, and temperature will change these results, as shown in a series of sensitivity analyses (Fig. 3 *D*–*F*). Here we document high and low estimates of atmospheric oxygen with variations in water age–depth distributions (*Supporting Information*), temperature (present day and +10 °C), and organic matter reactivity as revealed in the high, low, and combined sediment trap data. Higher water temperatures, as might be expected during this apparently ice-free time in Earth history, yield higher estimates for minimum atmospheric oxygen levels, whereas lower water ages yield lower estimates. We view 10 y as a conservative minimum water age; this is less than or equal to the water age found in the modern open ocean at water depths of >100 m, and similar to or less than those found in modern semienclosed basins (see *Supporting Information*). Higher organic matter reactivity (Fig. 3*F*) produces higher oxygen estimates, whereas lower reactivity (Fig. 3*D*) produces lower estimates.

With a water age of 10 y, minimum oxygen estimates range from 1.3% PAL (low reactivity, high latitude, Fig. 3*D*) to 6.2% PAL (high reactivity, low latitude, Fig. 3*F*) with 3.8% PAL for the combined data (Fig. 3*E*). As temperature is considered the prime variable controlling the latitudinal distribution of organic matter reactivities, and because the Xiamaling Formation deposited in a low-latitude setting, we favor the model results from the combined or low-latitude reactivities. Therefore, our sensitivity analysis reveals 3.8–6.2% PAL as a likely minimum atmospheric oxygen level, whereas 1.3% PAL is an unlikely but possible minimum estimate.

Our most likely minimum estimate of 3.8–6.2% PAL is very different from the <0.1% PAL oxygen suggested for this time from Cr isotope results (11). This result arises, ultimately, from a general lack

of fractionated Cr (with δ^{53}Cr values in the range of –0.25‰ to 0‰, compared with crustal values estimated at –0.1‰ to –0.2‰) in pre-Neoproterozoic iron-enriched marine sediments. Fractionations are imparted during the oxidative weathering of Cr(III) minerals on land, and fractionated Cr is transported to the sea and is believed to be captured in the iron-enriched sediments (40). Therefore, no fractionation would indicate no oxidative weathering on land and low levels of atmospheric oxygen. We note, however, that other data sets report evidence for fractionated Cr in pre-Neoproterozoic sediments, and, in particular, many banded iron formations in the time window from 1,800 Ma to 3,000 Ma have δ^{53}Cr values ranging up to 0.2–0.3‰ (40, 41). The discrepancy between these data sets has yet to be evaluated, but we note that no standard procedures are used to correct for a detrital Cr component. Therefore, we believe that the terrestrial and marine geochemical behavior of Cr is still poorly understood, and, in particular, it is unclear how chromium isotope signals are transferred from the land to marine sediments and which sediments best preserve such isotope signals.

Consequences of Elevated Mesoproterozoic Oxygen Levels

Atmospheric oxygen levels of 3.8–6.2% PAL (or even 1.3% PAL) are sufficient to support the respiration of sponges, considered good candidates for early evolved animals, whose oxygen requirements are in the range of ≤1–4% PAL (12). Such levels are also sufficient to support small motile animals such as annelid worms, which may require even less oxygen (13). Thus, it appears that sufficient oxygen existed to support animal metabolism long before the evolution of stem-group animals themselves, which, as noted above, from molecular phylogenetic evidence, occurred around 780 Ma (13). Thus, our results support the idea that oxygen itself did not limit the late emergence of animal life (1, 42).

ACKNOWLEDGMENTS. We thank Yu Wang, Caiyun Wei, Huitong Wang, Dina Holmgaard Skov, Heidi Grøn Jensen, Susanne Møller, Jørgen Kystol, and Anne Thoisen for technical support. We thank the Danish National Research Foundation (Grant DNRF53), the ERC (Oxygen Grant 267233), Danish Agency for Science, Technology and Innovation (Grant 12-125692), the Scientific Research and Technological Development Project of China National Petroleum Corporation (CNPC 2014A-0200 and CNPC 2014E-3209), and the State Key Program of National Natural Science Foundation of China (41530317).

1. Canfield DE (2014) *Oxygen: A Four Billion Year History* (Princeton Univ Press, Princeton, NJ).
2. Pavlov AA, Kasting JF (2002) Mass-independent fractionation of sulfur isotopes in Archean sediments: Strong evidence for an anoxic Archean atmosphere. *Astrobiology* 2(1):27–41.
3. Berner RA, Canfield DE (1989) A new model for atmospheric oxygen over Phanerozoic time. *Am J Sci* 289(4):333–361.
4. Berner RA (2006) GEOCARBSULF: A combined model for Phanerozoic atmospheric O_2 and CO_2. *Geochim Cosmochim Acta* 70(23):5653–5664.
5. Bergman NM, Lenton TM, Watson AJ (2004) COPSE: A new model of biogeochemical cycling over Phanerozoic time. *Am J Sci* 304(5):397–437.
6. Erwin DH, Valentine JW (2013) *The Cambrian Explosion: The Construction of Animal Biodiversity* (Roberts and Co, Greenwood Village, CO).
7. dos Reis M, et al. (2015) Uncertainty in the timing of origin of animals and the limits of precision in molecular timescales. *Curr Biol* 25(22):2939–2950.
8. Nursall JR (1959) Oxygen as a prerequisite to the origin of the metazoa. *Nature* 183(4669):1170–1172.
9. Berkner LV, Marshall LC (1965) On the origin and rise of oxygen concentration in the Earth's atmosphere. *J Atmos Sci* 22(3):225–261.
10. Mills DB, Canfield DE (2014) Oxygen and animal evolution: Did a rise of atmospheric oxygen "trigger" the origin of animals? *BioEssays* 36(12):1145–1155.
11. Planavsky NJ, et al. (2014) Earth history. Low mid-Proterozoic atmospheric oxygen levels and the delayed rise of animals. *Science* 346(6209):635–638.
12. Mills DB, et al. (2014) Oxygen requirements of the earliest animals. *Proc Natl Acad Sci USA* 111(11):4168–4172.
13. Sperling EA, et al. (2013) Oxygen, ecology, and the Cambrian radiation of animals. *Proc Natl Acad Sci USA* 110(33):13446–13451.
14. Zhang SH, et al. (2012) Pre-Rodinia supercontinent Nuna shaping up: A global synthesis with new paleomagnetic results from North China. *Earth Planet Sci Lett* 353: 145–155.
15. Meng QR, Wei HH, Qu YQ, Ma SX (2011) Stratigraphic and sedimentary records of the rift to drift evolution of the northern North China craton at the Paleo- to Mesoproterozoic transition. *Gondwana Res* 20(1):205–218.
16. Zhang S, et al. (2015) Orbital forcing of climate 1.4 billion years ago. *Proc Natl Acad Sci USA* 112(12):E1406–E1413.
17. Nameroff TJ, Balistrieri LS, Murray JW (2002) Suboxic trace metal geochemistry in the eastern tropical North Pacific. *Geochim Cosmochim Acta* 66(7):1139–1158.
18. Emerson SR, Huested SS (1991) Ocean anoxia and the concentrations of molybdenum and vanadium in seawater. *Mar Chem* 34(3-4):177–196.
19. Morford JL, Emerson SR, Breckel EJ, Kim SH (2005) Diagenesis of oxyanions (V, U, Re, and Mo) in pore waters and sediments from a continental margin. *Geochim Cosmochim Acta* 69(21):5021–5032.
20. Morford JL, Emerson S (1999) The geochemistry of redox sensitive trace metals in sediments. *Geochim Cosmochim Acta* 63(11-12):1735–1750.
21. Scholz F, et al. (2011) Early diagenesis of redox-sensitive trace metals in the Peru upwelling area—Response to ENSO-related oxygen fluctuations in the water column. *Geochim Cosmochim Acta* 75(22):7257–7276.
22. Brumsack HJ (2006) The trace metal content of recent organic carbon-rich sediments: Implications for Cretaceous black shale formation. *Palaeogeogr Palaeocl* 232(2-4): 344–361.
23. Piper DZ, Dean WE (2002) *Trace-Element Deposition in the Cariaco Basin, Venezuela Shelf, Under Sulfate-Reducing Conditions—A History of the Local Hydrography and Global Climate, 20 Ka to the Present* (US Geol Surv, Washington, DC).
24. Sperling EA, et al. (2014) Redox heterogeneity of subsurface waters in the Mesoproterozoic ocean. *Geobiology* 12(5):373–386.
25. Brocks JJ, Summons RE (2004) Sedimentary hydrocarbons, biomarkers for early life. Biogeochemistry, *Treatise on Geochemistry*, eds Holland HD, Turekian KK (Elsevier, Amsterdam), Vol 8, pp 64–115.
26. Overmann J (1992) Phylum BXI. Chlorobi phy. nov. Family I. "Chlorobiaceae" Green sulfur bacteria. *Bergey's Manual of Systematic Bacteriology*, eds Boone DR, Castenholz RW, Garrity GM (Springer, New York), 2nd Ed, Vol I, pp 601–604.
27. Repeta DJ (1993) A high-resolution historical record of Holocene anoxygenic primary production in the Black Sea. *Geochim Cosmochim Acta* 57(17):4337–4342.
28. Brocks JJ, et al. (2005) Biomarker evidence for green and purple sulphur bacteria in a stratified Palaeoproterozoic sea. *Nature* 437(7060):866–870.
29. Widdel F, et al. (1993) Ferrous iron oxidation by anoxygenic phototrophic bacteria. *Nature* 362:834–835.
30. Crowe SA, et al. (2008) Photoferrotrophs thrive in an Archean Ocean analogue. *Proc Natl Acad Sci USA* 105(41):15938–15943.
31. Koopmans MP, Schouten S, Kohnen MEL, Damste JSS (1996) Restricted utility of aryl isoprenoids as indicators for photic zone anoxia. *Geochim Cosmochim Acta* 60(23): 4873–4876.
32. Canfield DE, Kristensen E, Thamdrup B (2005) *Aquatic Geomicrobiology* (Academic, San Diego).
33. Luyten JR, Pedlosky J, Stommel H (1983) The ventilated thermocline. *J Phys Oceanogr* 13(2):292–309.
34. Karstensen J, Stramma L, Visbeck M (2008) Oxygen minimum zones in the eastern tropical Atlantic and Pacific oceans. *Prog Oceanogr* 77(4):331–350.
35. Canfield DE (2014) Proterozoic atmospheric oxygen. *The Atmosphere—History, Treatise on Geochemistry*, ed Farquhar J (Springer, Amsterdam), 2nd Ed, Vol 6, pp 197–216.
36. Logan GA, Hayes JM, Hieshima GB, Summons RE (1995) Terminal Proterozoic reorganization of biogeochemical cycles. *Nature* 376(6535):53–56.
37. Guidi L, et al. (2009) Effects of phytoplankton community on production, size and export of large aggregates: A world-ocean analysis. *Limnol Oceanogr* 54(6):1951–1963.
38. Richardson TL, Jackson GA (2007) Small phytoplankton and carbon export from the surface ocean. *Science* 315(5813):838–840.
39. Marsay CM, et al. (2015) Attenuation of sinking particulate organic carbon flux through the mesopelagic ocean. *Proc Natl Acad Sci USA* 112(4):1089–1094.
40. Frei R, Gaucher C, Poulton SW, Canfield DE (2009) Fluctuations in Precambrian atmospheric oxygenation recorded by chromium isotopes. *Nature* 461(7261):250–253.
41. Crowe SA, et al. (2013) Atmospheric oxygenation three billion years ago. *Nature* 501(7468):535–538.
42. Butterfield NJ (2011) Animals and the invention of the Phanerozoic Earth system. *Trends Ecol Evol* 26(2):81–87.
43. Gao LZ, et al. (2008) Mesoproterozoic age for Xiamaling Formation in North China Plate indicated by zircon SHRIMP dating. *Chin Sci Bull* 53(17):2665–2671.
44. US Geological Survey (1997) Reference material BCR-2: Basalt Columbia River. Available at crustal.usgs.gov/geochemical_reference_standards/basaltbcr2.html. Accessed October 2015.
45. US Geological Survey (1997) Reference material CLB-1: Coal, Lower Bakerstown. Available at crustal.usgs.gov/geochemical_reference_standards/coal.html. Accessed October 2015.
46. US Geological Survey (2014) Reference material SGR-1b: Oil shale, Green river shale. Available at crustal.usgs.gov/geochemical_reference_standards/shale.html#certinfo. Accessed October 2015.
47. National Research Council of Canada (1997) Reference material PACS-2: Harbour Sediment. Available at www.nrc-cnrc.gc.ca/eng/solutions/advisory/crm/certificates/hiss_1_mess_3_pacs_2.html. Accessed October 2013.
48. Lenniger M, Nohr-Hansen H, Hills LV, Bjerrum CJ (2014) Arctic black shale formation during Cretaceous Oceanic Anoxic Event 2. *Geology* 42(9):799–802.
49. Dahl TW, et al. (2013) Tracing euxinia by molybdenum concentrations in sediments using handheld X-ray fluorescence spectroscopy (HHXRF). *Chem Geol* 360-361: 241–251.
50. Rasmussen B, Fletcher IR, Brocks JJ, Kilburn MR (2008) Reassessing the first appearance of eukaryotes and cyanobacteria. *Nature* 455(7216):1101–1104.

51. Luo GM, Hallmann C, Xie SC, Ruan XY, Summons RE (2015) Comparative microbial diversity and redox environments of black shale and stromatolite facies in the Mesoproterozoic Xiamaling Formation. *Geochim Cosmochim Acta* 151:150–167.
52. Boning P, et al. (2004) Geochemistry of Peruvian near-surface sediments. *Geochim Cosmochim Acta* 68(21):4429–4451.
53. Lamborg CH, et al. (2008) The flux of bio- and lithogenic material associated with sinking particles in the mesopelagic "twilight zone" of the northwest and North Central Pacific Ocean. *Deep Sea Res Part II Top Stud Oceanogr* 55(14-15):1540–1563.
54. Middelburg JJ (1989) A simple rate model for organic-matter decomposition in marine-sediments. *Geochim Cosmochim Acta* 53(7):1577–1581.
55. Boudreau BP, Ruddick BR (1991) On a reactive continuum representation of organic matter diagenesis. *Am J Sci* 291(5):507–538.
56. Arndt S, Regnier P, Godderis Y, Donnadieu Y (2011) GEOCLIM reloaded (v 1.0): A new coupled Earth system model for past climate change. *Geosci. Model Dev.* 4(2):451–481.
57. Arndt S, et al. (2013) Quantifying the degradation of organic matter in marine sediments: A review and synthesis. *Earth Sci Rev* 123:53–86.
58. Buesseler KO, et al. (2009) Thorium-234 as a tracer of spatial, temporal and vertical variability in particle flux in the North Pacific. *Deep Sea Res Part I Oceanogr Res Pap* 56(7):1143–1167.
59. DeVries T, Deutsch C (2014) Large-scale variations in the stoichiometry of marine organic matter respiration. *Nat Geosci* 7(12):890–894.
60. Gamo T, et al. (2014) The Sea of Japan and its unique chemistry revealed by time-series observations over the last 30 years. *Monogr Environ. Earth Planets* 2(1):1–22.
61. Rudnick RL (2004) Composition of the continental crust. *The Crust, Treatise on Geochemistry*, ed Rudnick RL (Elsevier, Amsterdam), Vol 3, pp 1–64.
62. Key RM, et al. (2004) A global ocean carbon climatology: Results from Global Data Analysis Project (GLODAP). Global Biogeochem Cycles 18(4):GB4031.
63. Lüschen H (2004) Vergleichende anorganisch-geochemische Untersuchungen an phanerozoischen Corg-reichen Sedimenten: Ein Beitrag zur Charakterisierung ihrer Fazies. PhD dissertation (Univ Oldenburg, Oldenburg, Germany).
64. Calvert SE, Pedersen TF, Karlin RE (2001) Geochemical and isotopic evidence for post-glacial palaeoceanographic changes in Saanich Inlet, British Columbia. *Mar Geol* 174(1-4):287–305.
65. Dunne JP, Sarmiento JL, Gnanadesikan A (2007) A synthesis of global particle export from the surface ocean and cycling through the ocean interior and on the seafloor. Global Biogeochem Cycles 21(4):GB4006.
66. Takahata N, Sano Y, Horigucut K, ShiraO'and K, Ganio T (2008) Helium isotopes of seawater in the Japan Sea. *J Oceanogr* 64(2):293–301.
67. Lee BS, Bullister JL, Murray JW, Sonnerup RE (2002) Anthropogenic chlorofluorocarbons in the Black Sea and the Sea of Marmara. *Deep Sea Res Part I Oceanogr Res Pap* 49(5):895–913.
68. Sarma V (2002) An evaluation of physical and biogeochemical processes regulating perennial suboxic conditions in the water column of the Arabian Sea. *Global Biogeochem Cyles* 16(4):1082.
69. Olson DB, Hitchcock GL, Fine RA, Warren BA (1993) Maintenance of the low-oxygen layer in the central Arabian Sea. *Deep Sea Res Part II Top Stud Oceanogr* 40(3): 673–685.
70. Sarma VVSS (2002) An evaluation of physical and biogeochemical processes regulating the oxygen minimum zone in the water column of the Bay of Bengal. *Global Biogeochem Cycles* 16(4):1099.